



ORIGINAL RESEARCH

Open Access



^{18}F -C2Am: a targeted imaging agent for detecting tumor cell death in vivo using positron emission tomography

Flaviu Bulat^{1,2}, Friederike Hesse¹, De-En Hu¹, Susana Ros¹, Connor Willminton-Holmes², Bangwen Xie¹, Bala Attili¹, Dmitry Soloviev¹, Franklin Aigbirhio³, Finian. J. Leeper², Kevin M. Brindle¹  and André A. Neves^{1*} 

Abstract

Introduction: Trialing novel cancer therapies in the clinic would benefit from imaging agents that can detect early evidence of treatment response. The timing, extent and distribution of cell death in tumors following treatment can give an indication of outcome. We describe here an ^{18}F -labeled derivative of a phosphatidylserine-binding protein, the C2A domain of Synaptotagmin-I (C2Am), for imaging tumor cell death in vivo using PET.

Methods: A one-pot, two-step automated synthesis of N-(5- ^{18}F fluoropentyl)maleimide (60 min synthesis time, > 98% radiochemical purity) has been developed, which was used to label the single cysteine residue in C2Am within 30 min at room temperature. Binding of ^{18}F -C2Am to apoptotic and necrotic tumor cells was assessed in vitro, and also in vivo, by dynamic PET and biodistribution measurements in mice bearing human tumor xenografts treated with a TRAILR2 agonist or with conventional chemotherapy. C2Am detection of tumor cell death was validated by correlation of probe binding with histological markers of cell death in tumor sections obtained immediately after imaging.

Results: ^{18}F -C2Am showed a favorable biodistribution profile, with predominantly renal clearance and minimal retention in spleen, liver, small intestine, bone and kidney, at 2 h following probe administration. ^{18}F -C2Am generated tumor-to-muscle (T/m) ratios of 6.1 ± 2.1 and 10.7 ± 2.4 within 2 h of probe administration in colorectal and breast tumor models, respectively, following treatment with the TRAILR2 agonist. The levels of cell death (CC3 positivity) following treatment were 12.9–58.8% and 11.3–79.7% in the breast and colorectal xenografts, respectively. Overall, a 20% increase in CC3 positivity generated a one unit increase in the post/pre-treatment tumor contrast. Significant correlations were found between tracer uptake post-treatment, at 2 h post-probe administration, and histological markers of cell death (CC3: Pearson $R = 0.733$, $P = 0.0005$; TUNEL: Pearson $R = 0.532$, $P = 0.023$).

Conclusion: The rapid clearance of ^{18}F -C2Am from the blood pool and low kidney retention allowed the spatial distribution of cell death in a tumor to be imaged during the course of therapy, providing a rapid assessment of tumor treatment response. ^{18}F -C2Am has the potential to be used in the clinic to assess early treatment response in tumors.

Keywords: Cell death, PET, C2Am, Synaptotagmin-I, Tumor, TRAILR2

Introduction

The aim of cancer treatment, whether this is chemo-, radio-, targeted- or immuno-therapy [1], is to induce tumor cell death, where the two dominant forms of cell death are apoptosis and necrosis [2]. Cell death is an important and generic target for imaging early treatment response [3]. However, despite a long-standing unmet

*Correspondence: andre.neves@cruk.cam.ac.uk

¹ Cancer Research UK Cambridge Institute, Li Ka Shing Centre, University of Cambridge, Robinson Way, Cambridge CB2 0RE, UK

Full list of author information is available at the end of the article

need there are still no reliable techniques for routine imaging of cell death in the clinic [4].

Phosphatidylserine (PS) is externalized on the cell surface during apoptosis and is also exposed via the permeabilization of the plasma membrane that occurs during necrosis. The C2A domain of Synaptotagmin-1 binds PS in a calcium-dependent manner with nanomolar affinity [5, 6]. We have developed a PS-targeted imaging agent based on C2A, which was first used in vivo as a glutathione S-transferase-tagged dimeric construct (GST-C2A, 84 kDa) for imaging tumor cell death using MRI, where the protein was labeled with superparamagnetic iron oxide nanoparticles [7] and subsequently with Gd³⁺ chelates [8]. This GST-tagged construct has also been labeled with a ^{99m}Tc-chelate for SPECT [9] and with fluorine-18 for PET [10].

Subsequently, we have used the much smaller (16-kDa) isolated C2A domain [6], which enables better target access and tissue clearance. Introduction of a single cysteine residue, distant from the PS-binding site, using site-directed mutagenesis (S78C; C2Am), allowed the production of chemically defined derivatives in which this single cysteine was labeled with imaging tags. A near infrared-labeled derivative showed a fourfold lower binding to viable cells in vitro than a similarly labeled Annexin-V and therefore improved specificity for detecting cell death [6]. Annexin-V is another PS-binding protein, which was tested in the clinic nearly two decades ago in the form of ^{99m}Tc-HYNIC-Annexin-V, but showed suboptimal pharmacokinetics and extensive non-specific binding [11, 12]. A subsequent derivative, ^{99m}Tc-rh-Annexin-V-128, showed a better biodistribution profile and targeting of cell death in vivo [13].

We recently evaluated derivatives of C2Am that had been labeled for photoacoustic imaging [14] and SPECT [15]. The latter were based on ^{99m}Tc and ¹¹¹In chelates and could detect tumor cell death in vivo within 2 h of administration, with a tumor-to-muscle contrast of ~ 3. However, they also showed significant renal retention (>150% IA/g), which persisted for up to 24 h post-administration.

Here, we describe a ¹⁸F-labeled derivative of C2Am that was tested in human xenograft models of advanced colorectal (Colo205 [16]) and triple-negative breast (MDA-MB-231 [17]) cancer, treated with either conventional chemotherapy or with MEDI3039, which is a multivalent tumor necrosis factor (TNF)-related apoptosis-inducing ligand receptor-2 (TRAILR2) agonist that can induce tumor cell death at picomolar concentrations [18]. We analyzed the biodistribution and dosimetry profile of the probe and its sensitivity for detecting tumor cell death by correlating probe distribution in tumors with histological markers of tumor cell death in tumor sections.

Non-specific retention of the probe was evaluated by comparing its distribution with that of a site-directed mutant, ¹⁸F-iC2Am, which is inactive in PS binding [15].

Materials and methods

General

Details of the materials used including the precursor N-(5-[¹⁸F]fluoropentyl)maleimide and the imaging probe ¹⁸F-C2Am can be found in Additional file 1.

Cell culture

Chemicals were obtained from Sigma-Aldrich unless stated otherwise. MDA-MB-231 (ATCC, HTB-26TM) and Colo205 (ATCC, CCL-222TM) were purchased and stably transfected with firefly luciferase for bioluminescence imaging (BLI) using a method described previously [19], and used within ten passages from the original stocks. Both cell lines tested negative for mycoplasma and were authenticated using short-tandem repeat genetic profiling [20] yielding a 100% match to the cell lines in the ATCC database. MDA-MB-231 and Colo205 cells were cultured in DMEM or RPMI-1640 medium (Life Technologies), respectively, supplemented with 2 mmol/L L-glutamine and 10% fetal bovine serum (Life Technologies), in a humidified incubator at 37 °C and 5% CO₂.

Flow cytometry

Colo205 and MDA-MB-231 cells (2 million) were treated with 2.5 pM and 10 pM MEDI3039, respectively, for 24 h, centrifuged (700g, 5 min, 4 °C) and resuspended in 100 μL of pre-cooled HBS buffer (HEPES-buffered saline: 10 mmol/L HEPES, 150 mmol/L NaCl, 2 mmol/L CaCl₂, 1% fetal bovine serum (FBS), pH 7.4). Following incubation with SYTOX-Red (Invitrogen, 50 nM) and with C2Am-AF750 or AnnexinV-AF647 (conjugated to Alexa Fluor 750 or 647, respectively), at concentrations of 0.5 μM and 20 nM, respectively, the cells were washed twice, resuspended and kept on ice before analysis in a Symphony cytometer (Beckman), with 50,000 cells counted per event. Data were analyzed using FlowJo software (vs. 10) using methods described previously [6].

Cell labeling with ¹⁸F-C2Am

Vehicle- and MEDI3039-treated (10 pM, 24 h) cells (*n* = 3) were harvested, counted and viability assessed using a Vi-CELL analyzer (Beckman). The cells were then resuspended in HBS buffer and incubated with [¹⁸F]FPenM-C2Am (1–10 μM, 7–11 MBq, Am = ~ 10.5 GBq/μmol at the start of labeling) at 37 °C for 20 min. Cell pellets (5 million cells, centrifuged at 700g for 5 min at 4 °C) were washed three times with HBS buffer (1 mL) and radioactivity counted for 1 min using a gamma counter

(AMG Hidex) set to monitor the fluorine-18 gamma emission (511 keV).

Animal studies

Animal experiments were performed in compliance with a project license issued under the Animals (Scientific Procedures) Act of 1986 and were designed with reference to the UK Co-ordinating Committee on Cancer Research guidelines for the welfare of animals in experimental neoplasia [21]. Protocols were approved by the Cancer Research UK Cambridge Institute Animal Welfare and Ethical Review Body. Colo205 or MDA-MB-231 cells (5 or 10 million, respectively) were resuspended in 0.1 mL PBS or a 1:1 mixture of Matrigel (Corning) and complete DMEM, respectively, and implanted subcutaneously in the upper back of 10–12 week-old female BALB/c Nu/Nu mice (Charles River). Tumors were imaged when they reached $\sim 1 \text{ cm}^3$. For PET/CT imaging, mice were anesthetized using 1–2.5% isoflurane (Isoflo, Abbotts Laboratories Ltd.) in a 1:1 mixture of air and oxygen (at 1 L/min). MEDI3039, a TRAILR2 agonist, was administered at 0.1–0.4 mg/kg (i.v.) [22]. 5-fluorouracil (5FU) and doxorubicin (DOX) were used at 50–100 mg/kg (i.p.) and 100 mg/kg (i.p.), in the Colo205 and MDA-MB-231 models, respectively.

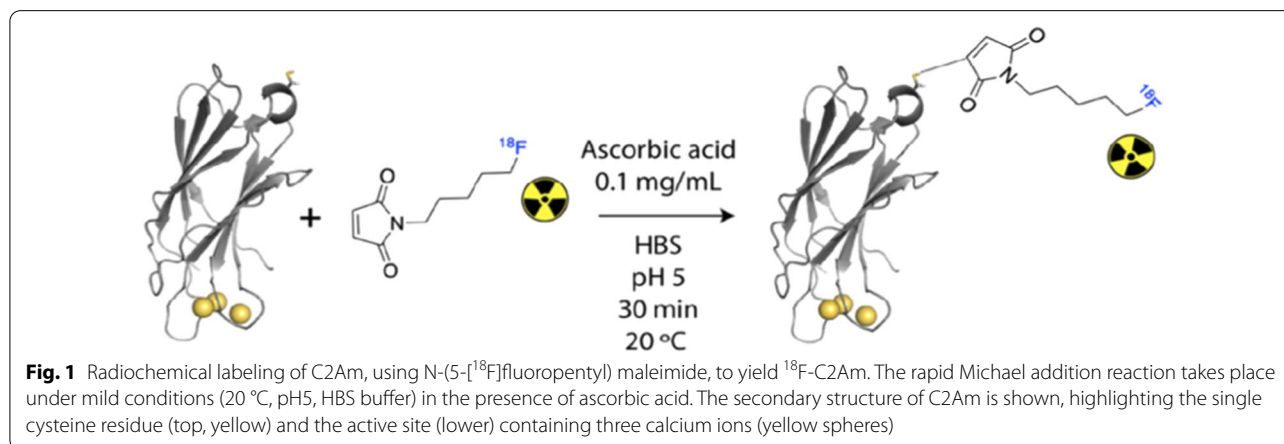
Production of ^{18}F -C2Am

A one-pot, two-step automated synthesis (Additional file 1: Fig. S1) of the prosthetic group N-(5- ^{18}F fluoropentyl) maleimide was developed using an automated module (GE TracerLab FxFN, 60 min synthesis time, >98% radiochemical purity and $12 \pm 3\%$ decay corrected yield, $n=3$; Additional file 1: Fig. S2). This was used to fully label the single cysteine residue in C2Am (Fig. 1) within 30 min at 20°C ($A_m = 212 \pm 30 \text{ GBq}/\mu\text{mol}$, >95% radiochemical purity, $n=3$, Fig. 1 and Fig. S3) to give ^{18}F -C2Am. Details on the radiosynthesis procedure,

quality control and radiometabolite analysis methods can be found in Additional file 1.

Dynamic ^{18}F -C2Am PET/CT imaging of treatment response
Colo205 ($n=9$) and MDA-MB231 ($n=9$) tumor-bearing mice underwent bioluminescence imaging (BLI) and PET-CT, following injection of ^{18}F -C2Am, which were performed in the same 2.5 h imaging session before and 24 h following treatment with MEDI3039 or chemotherapy (5FU or DOX, respectively). Following BLI, helical CT data were acquired for anatomical reference and attenuation correction (isotropic resolution of 0.2 mm). PET images, with a nominal isotropic resolution of 0.6 mm, were reconstructed using a 3D ordered subset expectation maximization (OSEM) method in one to three coincidence modes, eight iterations and six subsets. A 120-min dynamic PET acquisition was initiated 30 s prior to intravenous injection of $3.2 \pm 1.3 \text{ MBq } ^{18}\text{F}$ -C2Am ($150 \mu\text{g}/\text{kg}$; $10 \text{ mL}/\text{kg}$; $S_A = 1 \text{ MBq}/\mu\text{g}$), using a nanoScan PET/CT (Mediso) scanner. Scans were reconstructed into 23 time frames ($4 \times 15 \text{ s}$, from 0–1 min; $4 \times 1 \text{ min}$, 1–5 min; $11 \times 5 \text{ min}$, 5–60 min; $4 \times 15 \text{ min}$, 60–120 min). Images were normalized and corrected for decay and attenuation and analyzed using VivoQuant software (vs. 3, InviCRO). Three-dimensional tissue regions of interest (ROI) were drawn manually, and, if possible, Otsu thresholding was applied to better delineate the ROIs.

Standardized uptake values (SUV) were calculated as mean (SUV), median (SUV_{50}), the 90th percentile (SUV_{90}), peak (SUV_{peak}), peak_max ($\text{SUV}_{\text{peakM}}$) and maximum (SUV_{max}). SUV (g/mL) was defined as $\text{SUV} = C_{\text{img}} / (\text{IA}/\text{BW})$, where C_{img} is the activity concentration (MBq/mL) in the ROI, IA is the injected activity (MBq), and BW is the body weight of the animal (in grams). The pixel with the maximum signal intensity was used to calculate SUV_{max} . The fraction of injected activity per gram of tissue (IA/g, %), the tumor-to-muscle (T/m) and



tumor-to-blood (T/b) ratios were also calculated, the latter two using the lower flank skeletal muscle and carotid artery, respectively. Additional details are available in the Additional file 1.

Results

Flow cytometry of dying cells using C2Am-AF750

Following treatment with MEDI3039, MDA-MB-231 and Colo205 cells were predominantly necrotic (56.2%) or apoptotic (49.6%), respectively (Fig. 2a, b), based on cell membrane integrity, determined by Sytox Green staining, and the levels of NADH, which have been demonstrated previously as independent markers of these two modes of cell death [6]. Both cell lines upregulated expression of the TRAILR2 receptor upon treatment with the agonist (Additional file 1: Fig. S4). Necrotic and apoptotic cells showed greater mean fluorescence intensity (MFI) with C2Am-AF750 than viable cells, for both cell lines (Fig. 2c, d). Overall, the C2Am-AF750 MFI ratio for dead/viable cells (Fig. 2e, f, closed circles) at 24 h after treatment was similar for both cell lines (~ 10). Cell staining using Annexin-V (Fig. S5) indicated similar levels of apoptotic and necrotic cells, as those determined with C2Am, albeit the labeling of viable MDA-MB-231 and Colo205 cells using Annexin-V was greater than that observed for C2Am, as reported previously [6]. Incubation of ^{18}F -C2Am with the cells showed ~ 4 -fold greater retention of activity by MEDI3039-treated cells, in comparison with vehicle-treated control cells (see signal-to-background ratio (SBR) in Fig. 2g, h). The greater retention of ^{18}F -C2Am by MEDI3039-treated Colo205 cells (Fig. 2h) implies that there was greater exposure of PS in the predominantly apoptotic Colo205 cells as opposed to the predominantly necrotic MDA-MB-231 cells (Fig. 2a, b). Treatment of the Colo205 cells produced a large number of small apoptotic bodies ($\sim 8 \mu\text{m}$ vs $14 \mu\text{m}$ diameter for intact cells) and failure to fully capture these by centrifugation may have contributed to the variation observed in ^{18}F -C2Am retention in the cell pellets (Fig. 2h).

Biodistribution of ^{18}F -C2Am

Biodistribution was assessed in MEDI3039- and vehicle-treated control mice bearing Colo205 tumors (Fig. 3). Two hours following ^{18}F -C2Am administration most tissues showed low levels of activity ($< 2\%$ IA/g). Tumor activity post-treatment was at least ~ 2 -fold greater than in every other organ with the exception of kidney (the main clearance route). Renal retention ($\sim 6\%$ IA/g) was low and identical in both cohorts. The uptake of ^{18}F -C2Am was significantly higher ($P < 0.05$) in tumor, spleen and liver tissue following treatment, albeit the increase was smaller ($\sim 2.5 \times$) in spleen and liver, compared with tumor ($\sim 5 \times$) (Fig. 3). There was increased

cell death in the spleen ($P < 0.001$) and liver following MEDI3039 treatment, although the increase in the liver was not significant (Additional file 1: Fig. S6), which is likely due to low-level expression of TRAILR2 in these tissues [23]. The blood half-life of ^{18}F -C2Am, calculated from the analysis of dynamic data obtained from ROIs placed in the carotid artery, was 12.4 ± 2.2 min. ^{18}F -C2Am was stable in plasma for up to 8 h at 37°C (Additional file 1: Fig. S7) and was found to be intact in mouse blood in vivo at 15 min post-administration (Additional file 1: Fig. S8A), although by 30 min a lower molecular weight metabolite (< 3 kDa) had appeared and by 60 min approximately half of the radioactivity present was in this metabolite (Additional file 1: Fig. S8C-D). The same metabolite also appeared in the urine at 15 min and its concentration increased further at 30 and 60 min (Additional file 1: Fig. S8B, C-D), suggesting that there is some loss of the prosthetic group in vivo.

Dynamic PET imaging of tumor cell death using ^{18}F -C2Am

Dynamic PET imaging (Fig. 4a, b) confirmed renal excretion as the predominant clearance route for ^{18}F -C2Am. Bladder signal could be detected within 5–10 min of administration (Fig. 4a, b) and kidney cortical uptake peaked (at $\sim 40\%$ IA/g) within 20–30 min of injection (Fig. 4c, d, green line), but was minimal at 2 h post-administration ($\sim 3\%$ IA/g; Additional files 2, 3: videos 1 and 2). Tumor signal (Fig. 4a, b) could be detected within 15 min of injection, and there was a small component ($< 10\%$) of hepatobiliary clearance (Fig. 4c, d, blue line). Tumor-to-muscle (T/m) and tumor-to-blood (T/b) ratios were 10.7 ± 2.4 and 3.6 ± 0.5 , respectively, for MDA-MB-231 tumors and 6.1 ± 2.1 and 2.4 ± 0.4 , respectively, for Colo205 tumors, at 2 h post-administration of ^{18}F -C2Am. Analysis of individual tumors before and after treatment (Fig. 4e) showed significant increases in tumor retention (IA/g, %) of ^{18}F -C2Am at 1 h ($P < 0.005$) and 2 h ($P < 0.05$) post-administration, for both models. This significant difference ($P < 0.05$) between pre- and post-treatment ^{18}F -C2Am tumor uptake was also observed using SUV as the contrast metric (Fig. 4f). The tumor cells had been transduced with a viral vector expressing firefly luciferase prior to implantation, and both tumor models showed a significant decrease in bioluminescence ($P < 0.05$) post-treatment, where this decrease correlated with increased tumor uptake of ^{18}F -C2Am in MDA-MB-231 (IA/g, %) and in Colo205 (T/b) tumors (Fig. 4g). The levels of ^{18}F -C2Am tumor contrast (SUV and SUV_{max} ; Fig. S9), obtained 1 h post-administration, were 0.24 ± 0.14 and 0.66 ± 0.18 , respectively. There was a dose-dependent response to TRAIL2 agonist therapy in treated tumors for both models (Additional file 1: Fig. S10).

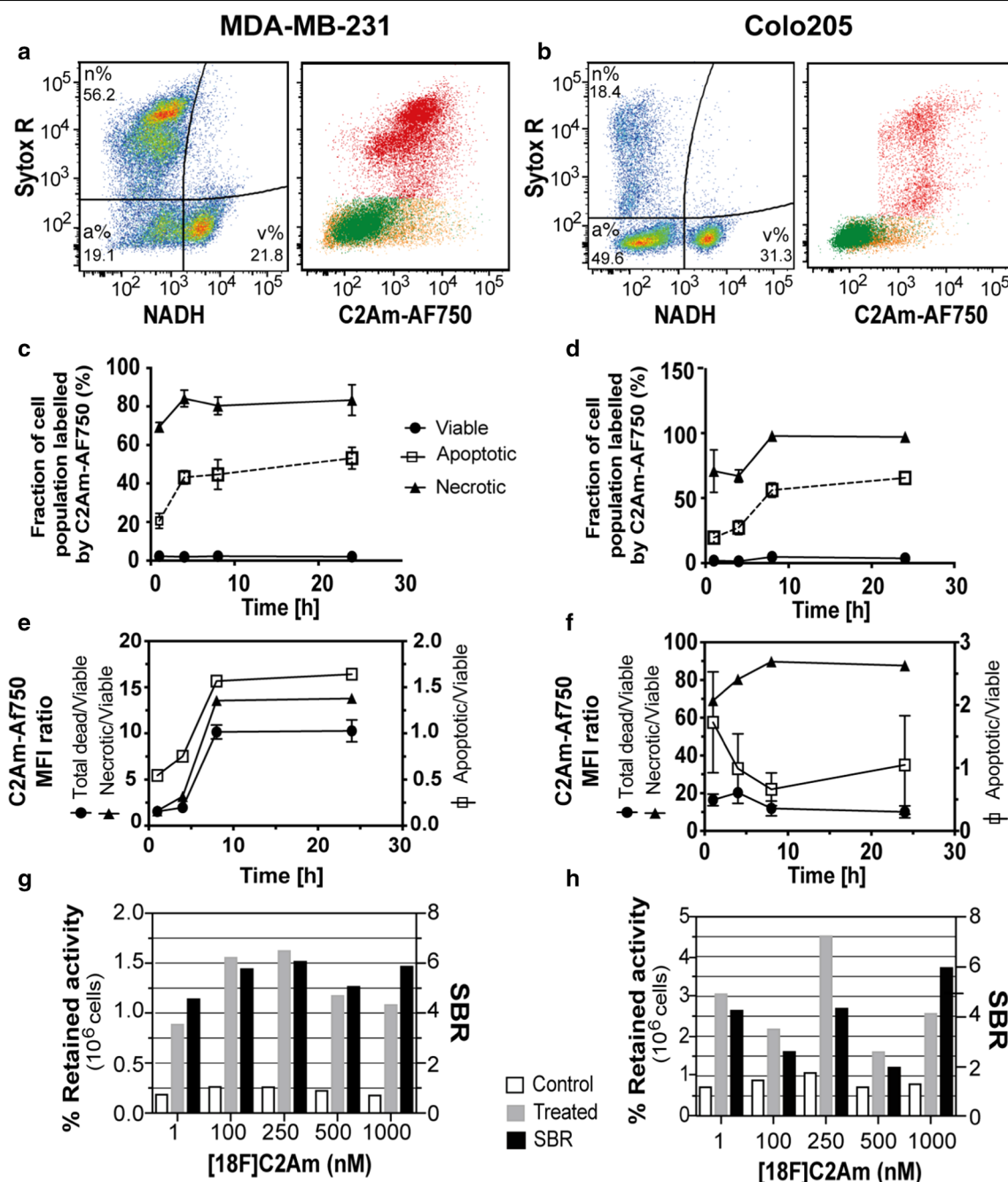
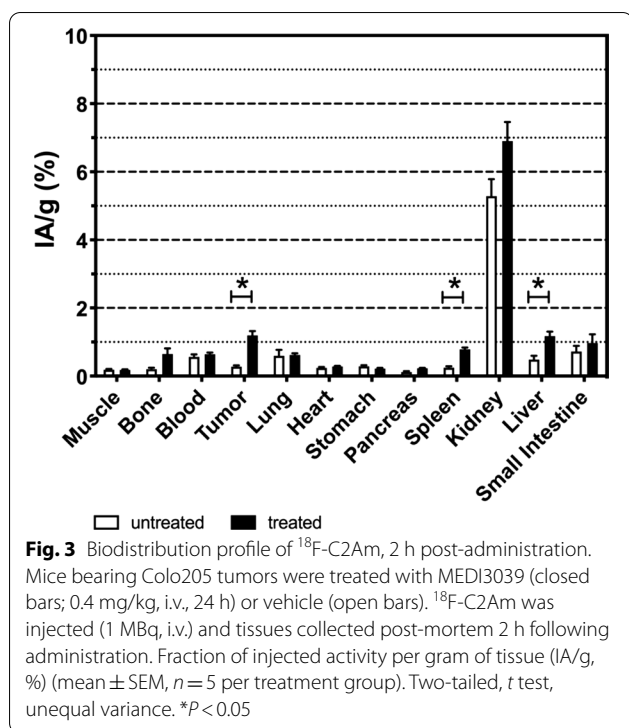


Fig. 2 C2Am binds to dead cells in vitro. Flow cytometric analysis of MEDI3039-treated MDA-MB-231 (a) and Colo205 (b) cells shows three distinct populations (first and third plots, from left), which were gated based on their levels of UV_A autofluorescence (NADH content) and plasma membrane integrity (Sytox R) as: viable (v%), apoptotic (a%) and necrotic (n%) cells. C2Am-AF750, a near infrared fluorophore-labeled derivative of C2Am labels (second and fourth plots) preferentially bound apoptotic (orange) and necrotic (red) cells, in comparison with viable (green) cells (c, d). Plots of C2Am-AF750 mean fluorescence intensity (MFI) ratios for necrotic/viable, apoptotic/viable and dead/viable MDA-MB-231 (e) and Colo205 (f) cells following treatment with MEDI3039 (mean ± SD, n = 3), error bars lie within the symbols when not shown. MEDI3039-treated MDA-MB-231 (g) and Colo205 (h) cells were incubated with ¹⁸F-C2Am at different concentrations (1–1000 nM) and the fraction of activity retained in the cell pellets (%) after three washes was measured. The signal-to-background ratio (SBR, black bars) of treated (grey bars) versus vehicle-treated (open bars, control) cells is also shown



Only ~ 15% of the contrast obtained with ¹⁸F-C2Am was observed with ¹⁸F-iC2Am (Fig. 5). Using unlabeled C2Am as a pre-blocking agent, at 10 × higher molar dose (1.5 mg/kg), generating a C2Am concentration of ~ 30 nM in the tumor, resulted in a ~ 70% decrease of ¹⁸F-C2Am retention in drug-treated tumors (Fig. 6c).

Correlation of ¹⁸F-C2Am with cell death markers

We analyzed several metrics of tumor contrast and their correlation with histological markers of tumor cell death in both the Colo205 and MDA-MB-231 tumor models (Fig. 7). IA/g (%), SUV, SUV₅₀ and T/b were found to best correlate with these cell death markers in both tumor models (Fig. 7a), particularly with cleaved caspase-3 staining (CC3, open bars; P < 0.05; R > 0.6). SUV₉₀ at 2 h post-probe administration correlated well with CC3 staining (Fig. 7a, P < 0.01, R > 0.6) but not with

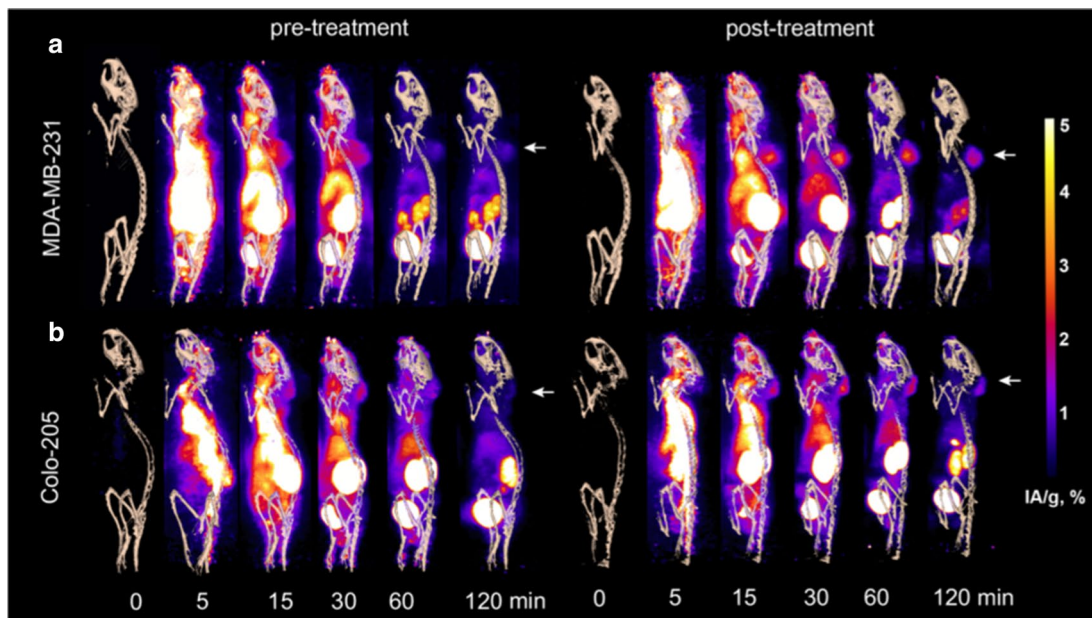
TUNEL (P > 0.05). Tumor contrast was also evaluated pre- and post-treatment for the same mice and expressed as ratios (post/pre-treatment) for IA/g (%), SUV or T/b (Fig. 7b). All three contrast metrics showed a good correlation with cleaved caspase-3 staining (CC3, %) in both tumor models, both at 1 h (P < 0.005; R > 0.62) and 2 h post-administration of ¹⁸F-C2Am (P < 0.03; R > 0.52). The slopes of the best fit lines for each metric, at 1 h or 2 h post-injection, were not significantly different. Overall, for all three metrics, a 20% increase in CC3 positivity resulted in a one unit increase in the post/pre-treatment tumor contrast. The correlation of ¹⁸F-C2Am tumor signal (expressed as %IA/g, SUV or T/b) post-treatment with CC3 positivity was in general better for the Colo205 model (0.69 < R < 0.86) than for the MDA-MB-231 model (0.47 < R < 0.68; Fig. S11). SUV_{max} showed a good correlation with CC3 positivity for MDA-MB-231 (R > 0.76) but not for Colo205 (R < 0.23; Additional file 1: Fig. S11). The correlation of the variation in ¹⁸F-C2Am tumor contrast with treatment (Additional file 1: Fig. S12) with CC3 positivity was better when expressed as ΔSUV (R = 0.694) than as ΔSUV_{max} (R = 0.567), 1 h after the injection of the contrast agent.

¹⁸F-C2Am signal in vivo and ex vivo versus histology

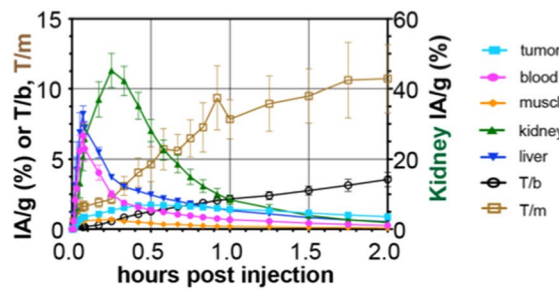
Next, we compared the percentage of the area occupied by dead cells on histology (CC3, %; Fig. 8a) with ¹⁸F-C2Am uptake in vivo (IA/g, %; Fig. 8b) and with the percentage of the area occupied by the ¹⁸F-C2Am signal in autoradiographs of excised tumor sections obtained following completion of the PET studies (Fig. 8c), 2 h post-administration of the imaging agent. Low levels of tumor cell death (CC3 < ~10%, Fig. 8a) generated low levels of ¹⁸F-C2Am retention, as detected by PET in vivo (IA/g, ~ 0.7%, Fig. 8b) and autoradiography ex vivo (~ 6%; Fig. 8c). Tumor PET and autoradiography signals increased significantly (IA/g, ~ 1.7%, P < 0.05) with the extent of tumor cell death commonly generated by conventional therapies (CC3 > ~ 20%,) [24]. ¹⁸F-C2Am signal in tumors post-treatment was heterogeneous in both models, as shown in multi-slice images from the tumors

(See figure on next page.)

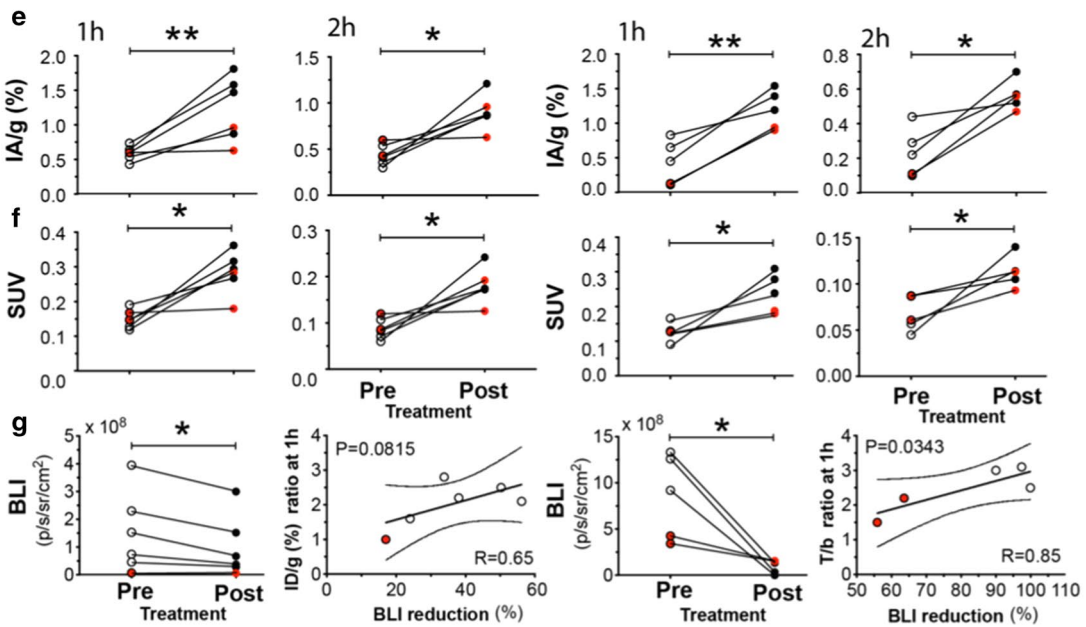
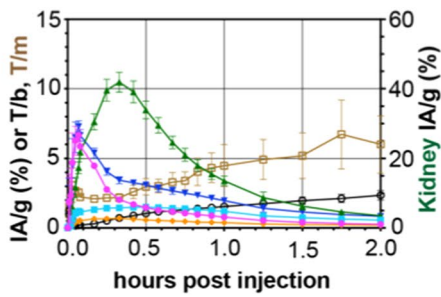
Fig. 4 PET images of ¹⁸F-C2Am in tumor-bearing mice, pre- and post-treatment. Maximum intensity projections of the PET signal in sagittal sections of representative mice, bearing MDA-MB-231 (a) and Colo205 (b) tumors. Projections are shown from immediately before (0) and up to 120 min after injection of ¹⁸F-C2Am. Signal is shown as injected activity per gram of tissue (IA/g, %) and overlaid on a CT-derived skeleton mask. White arrows indicate tumor location. Time-activity (IA/g, %) curves for the indicated tissues in treated (MEDI3039, 0.4 mg/kg, 24 h) MDA-MB-231 (c) and Colo205 (d) tumor-bearing mice. Also shown are tumor-to-blood (T/b) and tumor-to-muscle (T/m) ratios for both tumor models. e, f Pairwise analysis of PET signal pre- and 1 h (first and third columns) or 2 h (second and fourth columns) post-treatment, expressed as IA/g (%) (e) or SUV (f). Pairwise analysis (g) of tumor bioluminescence pre- and post-treatment (first and third plots) and correlation analysis (Pearson) of tumor PET signal with the reduction in BLI signal (second and fourth plots), 1 h after ¹⁸F-C2Am administration. Data (c, d) is mean ± SEM, n = 5–6 per treatment group. Black and red symbols (e, g) correspond to MEDI3039 treatment at 0.4 or 0.1 mg/kg (for 24 h), respectively. e, g Two-tailed, pairwise t test, unequal variance. *P < 0.05, **P < 0.01



c MDA-MB-231



d Colo205



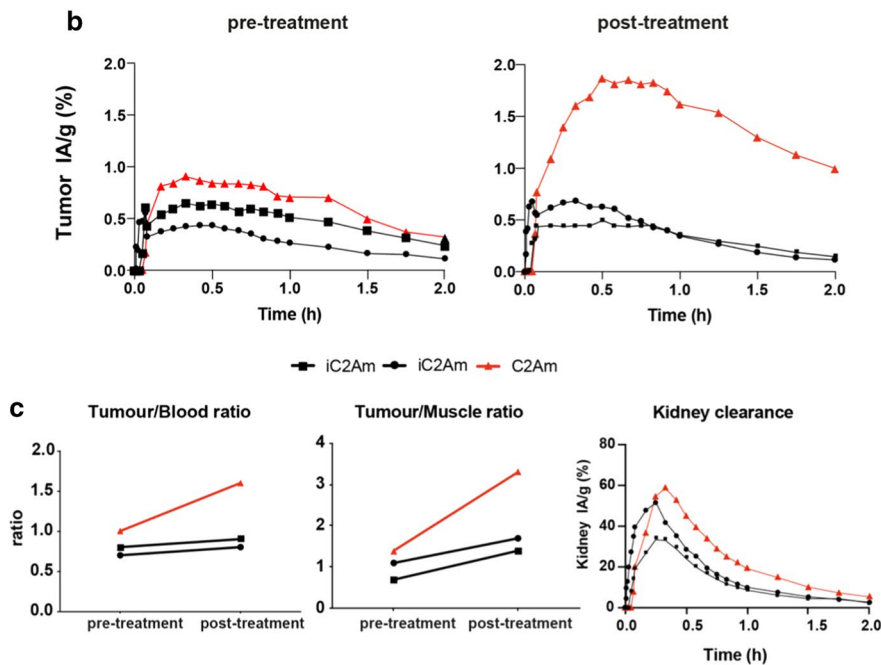
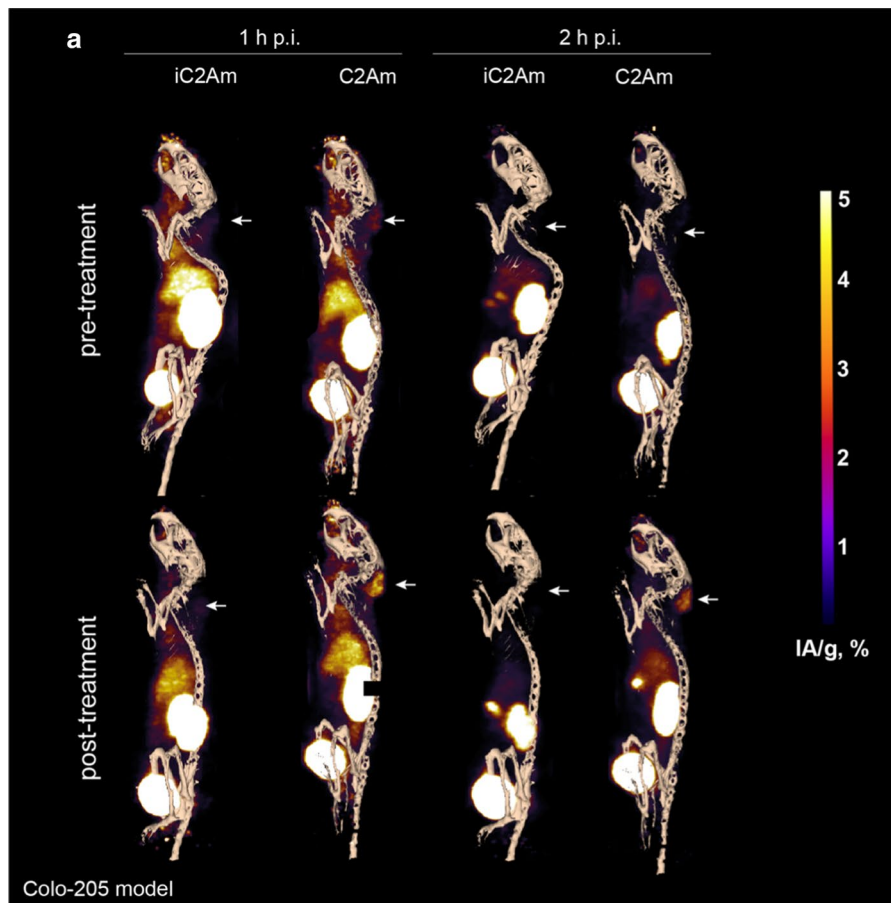


Fig. 5 Reduced tumor uptake of (inactive) ^{18}F -iC2Am versus (active) ^{18}F -C2Am in MEDI3039-treated mice (0.4 mg/kg, 24 h, i.v.) bearing Colo205 tumors. Red lined triangles (^{18}F -C2Am); black lined squares (^{18}F -iC2Am)

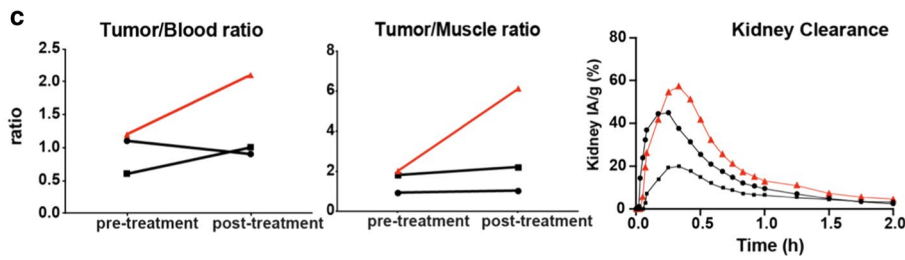
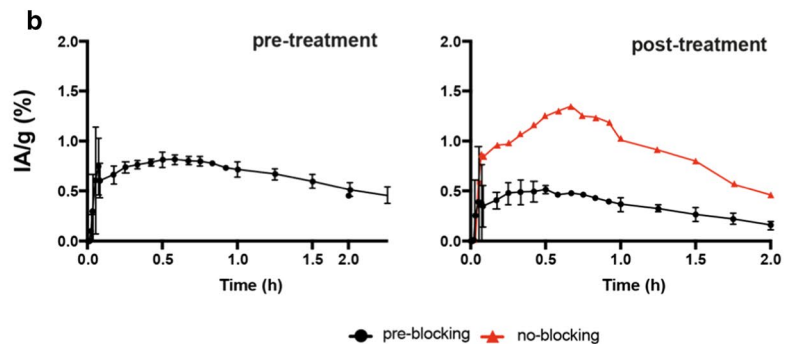
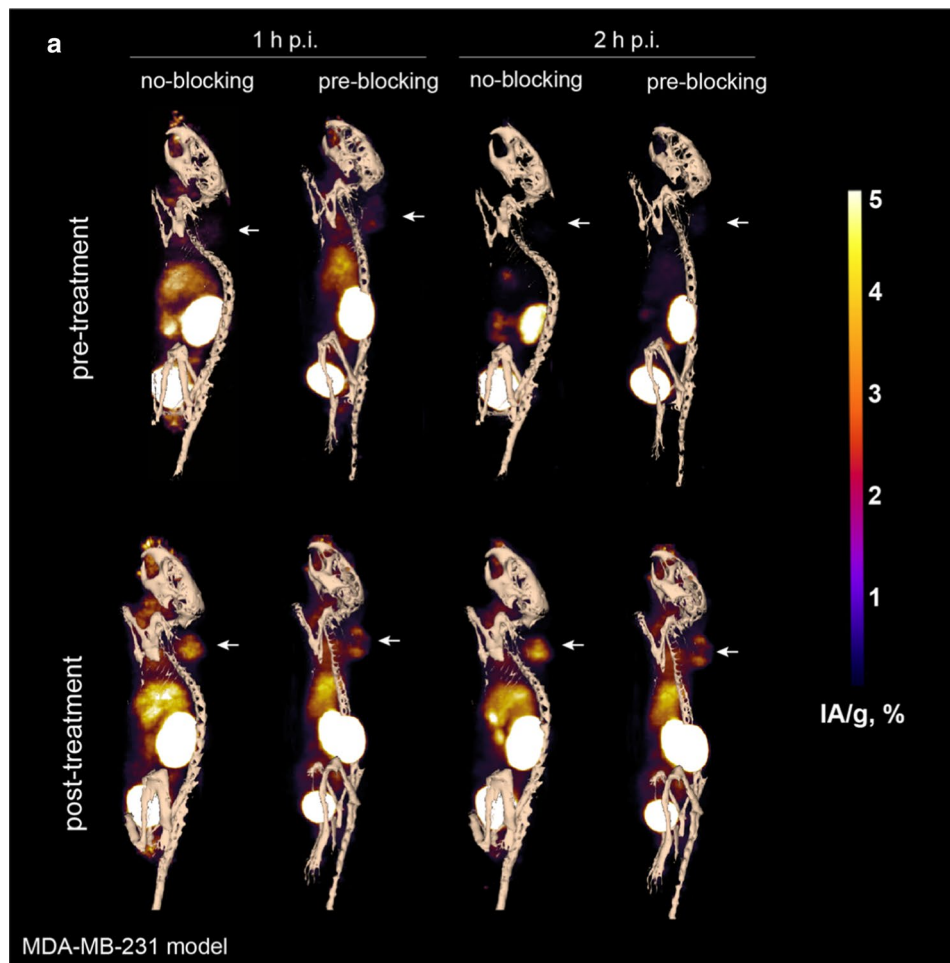


Fig. 6 Effect of pre-blocking of PS using ($\times 10$) molar excess of unlabeled C2Am on ^{18}F -C2Am tumor contrast in MEDI3039-treated mice (0.4 mg/kg, 24 h, i.v.) bearing MDA-MB-231 tumors. Red lined triangles (^{18}F -C2Am; no pre-blocking); black lined squares (^{18}F -C2Am; 10x pre-blocking with C2Am)

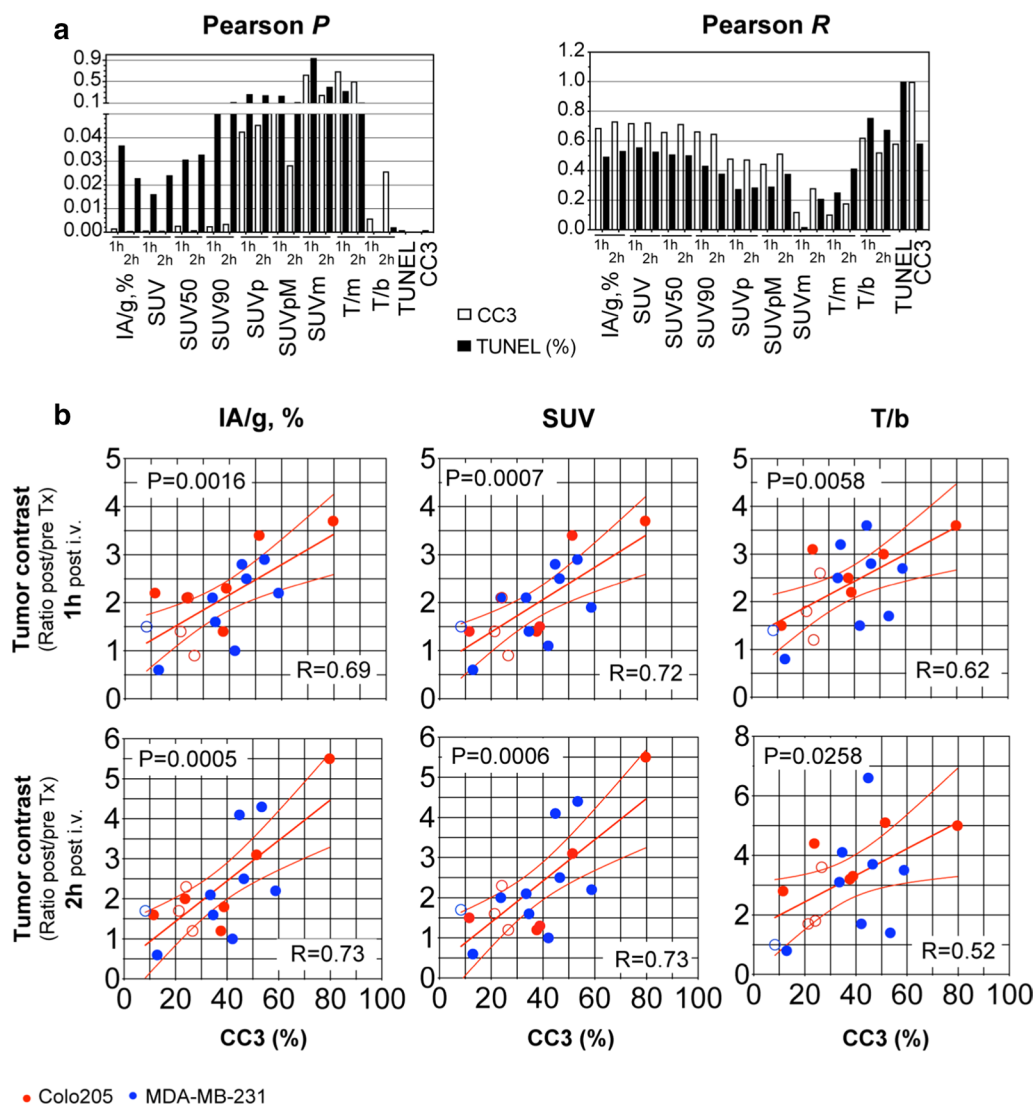


Fig. 7 Pearson correlation analysis of tumor PET signal with histological markers of cell death. **a** Pearson *P* (left) and *R* (right) correlation values for tumor signal, expressed as different contrast metrics, 1 h and 2 h post-administration of ^{18}F -C2Am, with cell death markers (CC3, open bars, or TUNEL, closed bars) estimated from two sections (200 μm apart) from the same tumors, from both Colo205 and MDA-MB-231 models. **(b)** Pearson correlation analysis of tumor contrast, expressed as IA/g, % (left), SUV (middle) and T/b ratio (right), 1 h (top row) or 2 h (lower row) after ^{18}F -C2Am administration, with tumor cell death (CC3, %). Tumor contrast is expressed as the signal ratio, post/pre-treatment. Pooled data **(a, b)** from Colo205 ($n=9$, red symbols) and MDA-MB-231 ($n=9$, blue symbols) tumor-bearing mice, treated with MED13039 (0.1 or 0.4 mg/kg, 24 h, i.v., filled symbols), 5FU (Colo205, 100 mg/kg, i.p., 24 h, open red symbols) or doxorubicin (MDA-MB-231, 100 mg/kg, i.p., 24 h, open blue symbols). Two-tailed, Pearson *P* and *R* values are shown **(a)**. CC3 cleaved caspase 3, TUNEL terminal deoxynucleotidyl transferase-mediated dUTP nick-end labeling. T/b tumor-to-blood ratio, Tx treatment

(Additional file 1: Fig. S13), reflecting the heterogeneous distribution of cell death observed on histology (Fig. 8a).

^{18}F -C2Am dosimetry

A dosimetry analysis was used to estimate the corresponding human dosimetry (Additional file 1: Table 1) using the interspecies scaling model proposed by Maina et al. [25] in order to examine the feasibility of

translating ^{18}F -C2Am into the clinic. ^{18}F -C2Am cleared from the mice rapidly with $27.3 \pm 6.1\%$ and $113.9 \pm 18\%$ of the injected radioactivity collecting in the bladder at one and 2 h after injection, respectively ($n=6$). The highest uptake was observed in the bladder, kidneys and liver. The estimated human-scaled effective dose was $12.5 \pm 5.7 \mu\text{Sv}/\text{MBq}$ (human effective dose estimate, in accordance with publication 103 of the

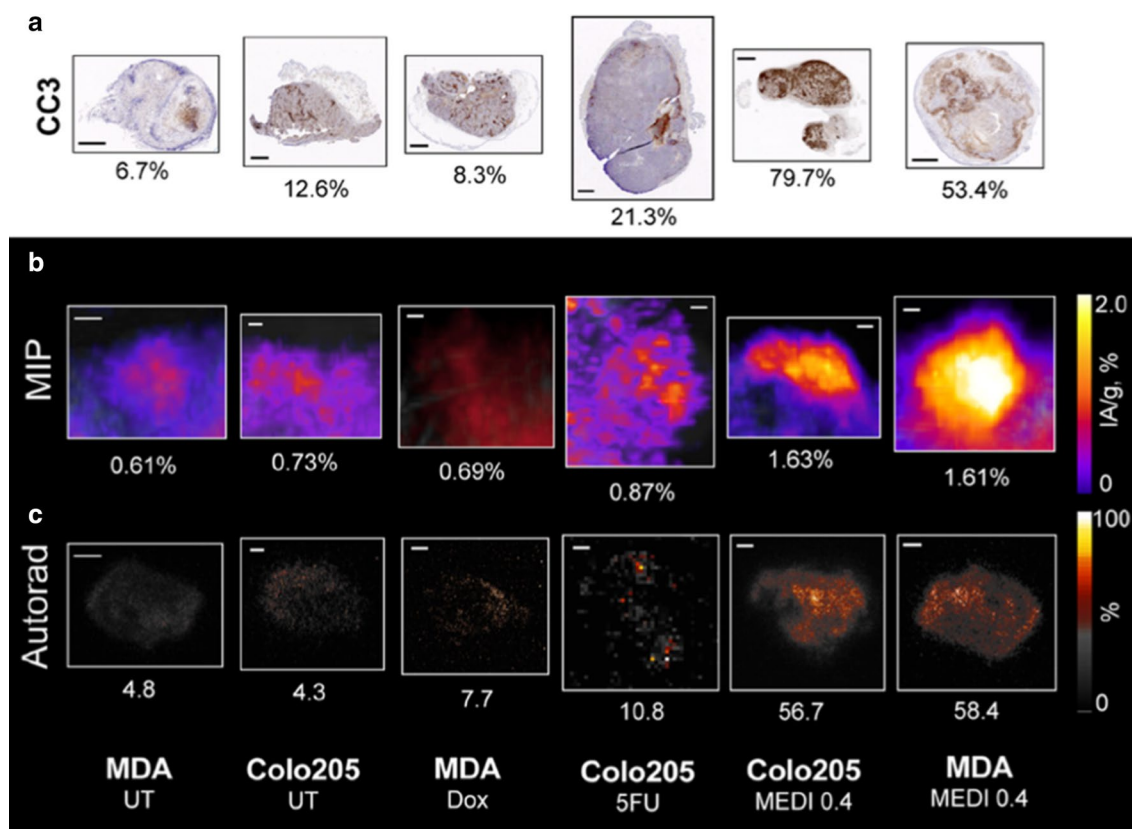


Fig. 8 Correlation of ^{18}F -C2A signal with immunohistochemical markers of cell death for representative MDA-MB-231 and Colo205 tumors. **a** Cleaved caspase-3 (CC3). Tumor section positive CC3 pixel count values (%) are shown. **b** Maximum intensity projection (MIP) of PET signal (IA/g, %). **c** Autoradiography of tumor sections acquired immediately after imaging (% of area with signal). Tumors were collected from different mice, bearing either Colo205 or MDA-MB-231, 2 h following administration of ^{18}F -C2Am. MEDI3039 (MEDI) used at 0.4 mg/kg, i.v., for 24 h. 5FU and Doxorubicin (Dox) were both used at 100 mg/kg, i.p., for 24 h. UT untreated tumors

International Commission on the Radiological Protection, ICRP [26]).

Discussion

Imaging cell death can provide an indication of disease prognosis [27] and in cancer can be used to detect treatment response [3, 28]. Imaging agents that target various cell death-related events, such as cleaved caspase-3 (CC3) [24], changes in mitochondrial membrane potential [29], alterations in membrane permeability [30] and exposure of PS [31] and phosphatidylethanolamine (PE) [32] have been described [28], some of which have translated to the clinic [33]. However, the success of these agents has so far been limited. A CC3 targeted agent, ^{18}F -ICMT-11, showed a lack of sensitivity for detecting cell death in breast and lung cancer patients treated with chemotherapy [34] and ^{18}F -ML-10, an agent that detects changes in membrane permeability during apoptosis, failed to detect response to chemotherapy in a pre-clinical model of breast cancer [35]. Exposure of PS [31]

and PE [32], which are externalized on the outer leaflet of the plasma membrane during apoptosis, or become accessible following plasma membrane disruption during necrosis, are attractive imaging targets since they provide a sustained and abundant target [14] that can give good image contrast [36]. $^{99\text{m}}\text{Tc}$ -Annexin V, which binds PS, has translated to the clinic; however, it showed poor pharmacokinetics and non-specific binding [33]. Exposure of PE by dying cells has been exploited in the development of duramycin, a 19 amino acid tetracyclic peptide (~2 kDa), as a cell death imaging agent [37, 38]. However, despite its smaller size the clearance profile and contrast generated by $^{99\text{m}}\text{Tc}$ -duramycin was similar to that observed here with ^{18}F -C2Am. Following treatment of Colo205 tumors with a TRAILR2 agonist, the increase in tumor-to-muscle (T/m) contrast generated by $^{99\text{m}}\text{Tc}$ -duramycin was $30.8 \pm 1.9 \times$ [37]. However, when corrected for non-specific retention using a control treatment antibody [37], the T/m was $6.9 \pm 1.5 \times$, which is similar to that observed here with ^{18}F -C2Am

($6.1 \pm 2.1 \times$). The retention of ^{18}F -iC2Am, which is non-specific, was $\sim 15\%$. More importantly, for clinical translation, ^{18}F -C2Am showed comparable blood half-life ($t_{1/2}$: 12.4 ± 2.2 min) to that reported recently for the small PET agent ^{68}Ga -duramycin ($t_{1/2}$: 17.3 ± 4.12 min) [39], but longer than that observed previously for the SPECT agent $^{99\text{m}}\text{Tc}$ -duramycin ($t_{1/2}$: 4.1 ± 0.3 min) [40]. Cell death-dependent contrast was obtained earlier using ^{18}F -C2Am, at 2 h following agent administration, as compared to 4 h for $^{99\text{m}}\text{Tc}$ -duramycin.

^{18}F -C2Am also cleared more quickly than the γ -emitter labeled C2Am derivatives described previously ($^{99\text{m}}\text{Tc}$ -C2Am, $t_{1/2}$: 582 ± 6 min; ^{111}In -C2Am, $t_{1/2}$: 480 ± 48 min) [15] and gave higher T/m ratios (~ 6 – $10 \times$) as compared to $^{99\text{m}}\text{Tc}$ -C2Am ($\sim 4.3 \times$) and ^{111}In -C2Am ($\sim 2.2 \times$), albeit with different tumor models (EL4 and Colo205) and treatment (chemotherapy) [15]. The C2Am fragment (< 3 kDa) detected in serum and urine, within 30 min of administration, is likely the result of proteolytic cleavage in the liver and/or kidney, which could contribute to this rapid clearance. The mean SUV_{max} for ^{18}F -C2Am at 1 h post-administration (0.66 ± 0.18) was greater than that reported previously for a much larger ^{18}F -labeled C2A derivative (^{18}F -GST-C2A; 80 kDa; $\text{SUV}_{\text{max}} = 0.47 \pm 0.28$) [10]. Moreover, no inactive C2A controls were performed in this previous study, suggesting that a substantial part of the tumor signal may have been caused by non-specific retention [10]. ^{18}F -C2Am showed greater T/m contrast (two- to threefold) for identical levels of cell death and lower (2–10 \times) non-specific retention in other tissues post-treatment when compared to ^{18}F -ICMT-11 [24], ^{18}F -ML-10 [35], $^{99\text{m}}\text{Tc}$ -Duramycin [36], and ^{18}F -Annexin V [41].

Pre-blocking PS using unlabeled C2Am at tenfold greater molar dose than ^{18}F -C2Am resulted in a $\sim 70\%$ reduction in tumor retention of ^{18}F -C2Am. This reduction was much greater than expected given the high levels of PS predicted to be exposed by dying cells in these tumors ($\sim 30 \mu\text{M}$), based on cell treatment experiments *in vitro* [14], and suggests that the PS accessible to C2Am *in vivo* is much less than this.

The levels of tumor cell death observed in the clinic can vary widely, from a few percent pre-treatment to 5–16% apoptosis following neoadjuvant treatment in breast cancer [42, 43]. ^{18}F -C2Am detects both apoptosis and necrosis and therefore should be more sensitive than those agents that detect apoptosis alone, such as ^{18}F -ML-10 [35]. Moreover, C2Am is also capable of binding PE [44], which like PS, is also externalized to the surface of dying cells.

The contrast observed here, where SUV doubled within an hour of ^{18}F -C2Am injection following an increase in cell death from 8 to 20%, suggests that this agent should

detect the expected levels of tumor cell death in the clinic. Analysis of ^{18}F -C2Am signal heterogeneity, for example using Minkowski functionals, which we have used previously to analyze the heterogeneous distribution of a gadolinium chelate-conjugated derivative of C2A in magnetic resonance images [45], could further enhance the sensitivity of the agent for detecting treatment response.

The estimated human mean effective dose with ^{18}F -C2Am is $12.5 \pm 5.7 \mu\text{Sv}/\text{MBq}$, which was higher than that estimated for the SPECT tracer $^{99\text{m}}\text{Tc}$ -duramycin ($3.19 \pm 2.16 \mu\text{Sv}/\text{MBq}$) [40], but similar to that observed recently for a small molecule PET tracer (^{18}F -PSMA-11; $12.8 \pm 0.6 \mu\text{Sv}/\text{MBq}$) [46], and for a biologic ($^{99\text{m}}\text{Tc}$ -Annexin-V; $9.7 \pm 1.0 \mu\text{Sv}/\text{MBq}$) [47]. The total estimated effective human dose of ^{18}F -C2Am equates to 5.6 ± 2.6 mSv (450 MBq injected), which is less than the PET element of a [^{18}F]FDG PET/CT scan, 9.0 ± 1.6 mSv [48].

In conclusion, we have demonstrated ^{18}F -C2Am as a PET agent for imaging cell death *in vivo* that showed fast renal clearance, good tumor contrast post-treatment and acceptable dosimetry. ^{18}F -C2Am has the potential to be used in the clinic to assess early treatment response in tumors, such as breast, prostate, lung and colorectal.

Supplementary Information

The online version contains supplementary material available at <https://doi.org/10.1186/s13550-020-00738-7>.

Additional file 1. Supporting methods and data.

Additional file 2. Supporting video 1.

Additional file 3. Supporting video 2.

Abbreviations

BLI: Bioluminescence imaging; CC3: Cleaved-caspase-3 histological assay for apoptosis; C2Am: C2A domain of Synaptotagmin-I; PS: Phosphatidylserine; TRAILR2: (TNF)-related apoptosis-inducing ligand receptor-2; TUNEL: Terminal deoxynucleotidyl transferase dUTP nick-end labeling (histological assay for necrosis).

Acknowledgements

We thank Istvan Boros, Tunde Miklovicz, Stefan Hader, Roberto Canales-Candela and Paul Burke, of the Radio Pharmacy Unit of the Wolfson Brain Imaging Centre, University of Cambridge, for facilitating access to the cyclotron and fluorine-18. We thank Franklin Aigbirio for providing the required instrumentation for radiochemical synthesis and his research group for stimulating discussion. We thank Sarah Heard and Daniel Gillet, of the Nuclear Medicine Department of Addenbrooke's Hospital Cambridge, for their advice on accessing IDAC 2.0 software. We thank David Lewis for his advice on VivoQuant analysis. We are grateful to Jodi Miller and Jo Arnold of the CRUK Cambridge Institute Histopathology Unit, and also to the Research Instrumentation, Imaging and Bioresources Units, for their support. We thank Robert Wilkinson and MedImmune for providing the TRAIL-R2 agonist (MEDI3039). We are grateful to Kelly Holmes and Sarah McGuire for their project management support.

Authors' contributions

AAN and KMB develop the concept and designed the study. ANN supervised the study. FB, FH, DH, SR, CWH, BX, BA, DS, FA, FL and AAN developed

methodology. FB, FH, and AAN acquired data. FB, FH, KMB and AAN analyzed and interpreted data. AAN and KMB wrote, reviewed and edited the manuscript, with input from all authors who read and approved the final manuscript.

Funding

This work was supported by a Cancer Research U.K. Programme Grant to Kevin M. Brindle (17242) and by the CRUK-EPSCRC Imaging Centre in Cambridge and Manchester (16465). F. Bulat was the recipient of a Ph.D. fellowship studentship from the CRUK-EPSCRC programme.

Availability of data and materials

The datasets used and/or analyzed during the current study are available at <https://doi.org/10.17863/CAM.60617>.

Ethics approval and consent to participate

All applicable institutional and/or national guidelines for the care and use of animals were followed, and the study protocol was approved by the institutional Research Ethics Board.

Consent for publication

Not applicable.

Competing interests

C2Am is under a licensing agreement with Cambridge Enterprise, and has been patented (US2011/0038798). Some of the authors of this study (André A. Neves and Kevin M. Brindle) are coinventors on this patent. No other potential conflict of interest relevant to this article was reported.

Author details

¹ Cancer Research UK Cambridge Institute, Li Ka Shing Centre, University of Cambridge, Robinson Way, Cambridge CB2 0RE, UK. ² Department of Chemistry, University of Cambridge, Cambridge CB2 1EW, UK. ³ Wolfson Brain Imaging Centre, University of Cambridge, Cambridge CB2 0QQ, UK.

Received: 27 July 2020 Accepted: 23 November 2020

Published online: 09 December 2020

References

- Falzone L, Salomone S, Libra M. Evolution of cancer pharmacological treatments at the turn of the third millennium. *Front Pharmacol*. 2018;9:1300.
- Nonnenmacher L, Hasslacher S, Zimmermann J, Karpel-Massler G, La Ferla-Brühl K, Barry SE, Burster T, Siegelin MD, Brühl O, Halatsch ME, Debatin KM, Westhoff MA. Cell death induction in cancer therapy—past, present, and future. *Crit Rev Oncog*. 2016;21:253–67.
- Neves AA, Brindle KM. Imaging cell death. *J Nucl Med*. 2014;55:1–4.
- Dean E, Greystoke A, Ranson M, Dive C. Biomarkers of cell death applicable to early clinical trials. *Exp Cell Res*. 2012;318:1252–9.
- Davletov B, Perisic O, Williams RL. Calcium-dependent membrane penetration is a hallmark of the C2 domain of cytosolic phospholipase A2 whereas the C2A domain of synaptotagmin binds membranes electrostatically. *J Biol Chem*. 1998;273:19093–6.
- Alam IS, Neves AA, Witney TH, Boren J, Brindle KM. Comparison of the C2A domain of Synaptotagmin-I and Annexin-V as probes for detecting cell death. *Bioconjug Chem*. 2010;21:884–91.
- Zhao M, Beauregard DA, Loizou L, Davletov B, Brindle KM, Technology NEW. Non-invasive detection of apoptosis using magnetic resonance imaging and a targeted contrast agent. *Nat Med*. 2001;7:1241–4.
- Krishnan AS, Neves AA, de Backer MM, Hu DE, Davletov B, Kettunen MI, Brindle KM. Detection of cell death in tumors by using MR imaging and a gadolinium-based targeted contrast agent. *Radiology*. 2008;246:854–62.
- Wang F, Fang W, Zhao M, Wang Z, Ji S, Li Y, Zheng Y. Imaging paclitaxel (chemotherapy)-induced tumor apoptosis with ^{99m}Tc C2A, a domain of Synaptotagmin I: a preliminary study. *Nucl Med Biol*. 2008;35:359–64.
- Wang F, Fang W, Zhang MR, Zhao M, Liu B, Wang Z, Hua Z, Yang M, Kumata K, Hatori A, Yamasaki T, Yamamoto K, Suzuki K. Evaluation of chemotherapy response in VX2 rabbit lung cancer with 18F-labeled C2A domain of synaptotagmin I. *J Nucl Med*. 2011;52:592–9.
- De Saint-Hubert M, Prinsen K, Mortelmans L, Verbruggen A, Mottaghy FM. Molecular imaging of cell death. *Methods*. 2009;48:178–87.
- Wang X, Feng H, Zhao S, Xu J, Wu X, Cui J, Zhang Y, Qin Y, Liu Z, Gao T, Gao Y, Zeng W. SPECT and PET radiopharmaceuticals for molecular imaging of apoptosis: from bench to clinic. *Oncotarget*. 2017;8:20476–95.
- Wuest M, Perreault A, Richter S, Knight JC, Wuest F. Targeting phosphatidylserine for radionuclide-based molecular imaging of apoptosis. *Apoptosis*. 2019;24:221–44.
- Xie B, Tomaszewski MR, Neves AA, Ros S, Hu DE, McGuire S, Mullins SR, Tice D, Sainson RCA, Bohndiek SE, Wilkinson RW, Brindle KM. Optoacoustic detection of early therapy-induced tumor cell death using a targeted imaging agent. *Clin Cancer Res*. 2017;23:6893–903.
- Neves AA, Xie B, Fawcett S, Alam IS, Witney TH, de Backer MM, Summers J, Hughes W, McGuire S, Soloviev D, Miller J, Howat WJ, Hu DE, Rodrigues TB, Lewis DY, Brindle KM. Rapid imaging of tumor cell death in vivo using the C2A domain of Synaptotagmin-I. *J Nucl Med*. 2017;58:881–7.
- Semple TU, Quinn LA, Woods LK, Moore GE. Tumor and lymphoid cell lines from a patient with carcinoma of the colon for a cytotoxicity model. *Cancer Res*. 1978;38:1345–55.
- Cailleau R, Young R, Olivé M, Reeves WJ. Breast tumor cell lines from pleural effusions. *J Natl Cancer Inst*. 1974;53:661–74.
- Swers JS, Grinberg L, Wang L, Feng H, Lekstrom K, Carrasco R, Xiao Z, Inigo I, Leow CC, Wu H, Tice DA, Baca M. Multivalent scaffold proteins as superagonists of TRAIL receptor 2-induced apoptosis. *Mol Cancer Ther*. 2013;12:1235–44.
- Patrick PS, Hammersley J, Loizou L, Kettunen MI, Rodrigues TB, Hu DE, Tee SS, Hesketh R, Lyons SK, Soloviev D, Lewis DY, Aime S, Fulton SM, Brindle KM. Dual-modality gene reporter for in vivo imaging. *Proc Natl Acad Sci U S A*. 2014;111:415–20.
- Schilling F, Ros S, Hu DE, D'Santos P, McGuire S, Mair R, Wright AJ, Mannion E, Franklin RJ, Neves AA, Brindle KM. MRI measurements of reporter-mediated increases in transmembrane water exchange enable detection of a gene reporter. *Nat Biotechnol*. 2017;35:75–80.
- Workman P, Aboagye EO, Balkwill F, Balmain A, Bruder G, Chaplin DJ, Double JA, Everitt J, Farningham DA, Glennie MJ, Kelland LR, Robinson V, Stratford IJ, Tozer GM, Watson S, Wedge SR, Eccles SA. Guidelines for the welfare and use of animals in cancer research. *Br J Cancer*. 2010;102:1555–77.
- Hesketh RL, Wang J, Wright AJ, Lewis DY, Denton AE, Grenfell R, Miller JL, Bielik R, Gehrung M, Fala M, Ros S, Xie B, Hu DE, Brindle KM. Magnetic resonance imaging is more sensitive than PET for detecting treatment-induced cell death-dependent changes in glycolysis. *Cancer Res*. 2019;79:3557–69.
- Finnberg NK, Gokare P, Navaraj A, Lang Kuhs KA, Cerniglia G, Yagita H, Takeda K, Motoyama N, El-Deiry WS. Agonists of the TRAIL death receptor DR5 sensitize intestinal stem cells to chemotherapy-induced cell death and trigger gastrointestinal toxicity. *Cancer Res*. 2016;76:700–12.
- Nguyen QD, Smith G, Glaser M, Perumal M, Arstad E, Aboagye EO. Positron emission tomography imaging of drug-induced tumor apoptosis with a caspase-3/7 specific [18F]-labeled isatin sulfonamide. *Proc Natl Acad Sci U S A*. 2009;106:16375–80.
- Maina T, Konijnenberg MW, KolencPeitl P, Garnuszek P, Nock BA, Kaloudi A, Kroselj M, Zalete K, Maecke H, Mansi R, Erba P, von Guggenberg E, Hubalewska-Dydejczyk A, Mikolajczak R, Decristoforo C. Preclinical pharmacokinetics, biodistribution, radiation dosimetry and toxicity studies required for regulatory approval of a phase I clinical trial with (111)In-CP04 in medullary thyroid carcinoma patients. *Eur J Pharm Sci*. 2016;91:236–42.
- Andersson M, Johansson L, Eckerman K, Mattsson S. IDAC-Dose 2.1, an internal dosimetry program for diagnostic nuclear medicine based on the ICRP adult reference voxel phantoms. *EJNMMI Res*. 2017;7:88.
- Wang KK, Yang Z, Zhu T, Shi Y, Rubenstein R, Tyndall JA, Manley GT. An update on diagnostic and prognostic biomarkers for traumatic brain injury. *Expert Rev Mol Diagn*. 2018;18:165–80.
- Rybczynska AA, Boersma HH, de Jong S, Gietema JA, Noordzij W, Dierckx RAJO, Elsinga PH, van Waarde A. Avenues to molecular imaging of dying cells: focus on cancer. *Med Res Rev*. 2018;38:1713–68.

29. Reshef A, Shirvan A, Shohami E, Grimberg H, Levin G, Cohen A, Trembovler V, Ziv I. Targeting cell death in vivo in experimental traumatic brain injury by a novel molecular probe. *J Neurotrauma*. 2008;25:569–80.
30. Oborski MJ, Laymon CM, Lieberman FS, Drappatz J, Hamilton RL, Mountz JM. First use of (18)F-labeled ML-10 PET to assess apoptosis change in a newly diagnosed glioblastoma multiforme patient before and early after therapy. *Brain Behav*. 2014;4:312–5.
31. Martin SJ, Reutelingsperger CP, McGahon AJ, Rader JA, van Schie RC, LaFace DM, Green DR. Early redistribution of plasma membrane phosphatidylserine is a general feature of apoptosis regardless of the initiating stimulus: inhibition by overexpression of Bcl-2 and Abl. *J Exp Med*. 1995;182:1545–56.
32. Elvas F, Stroobants S, Wyffels L. Phosphatidylethanolamine targeting for cell death imaging in early treatment response evaluation and disease diagnosis. *Apoptosis*. 2017;22:971–87.
33. Belhocine T, Steinmetz N, Hustinx R, Bartsch P, Jerusalem G, Seidel L, Rigo P, Green A. Increased uptake of the apoptosis-imaging agent (99m)Tc recombinant human Annexin V in human tumors after one course of chemotherapy as a predictor of tumor response and patient prognosis. *Clin Cancer Res*. 2002;8:2766–74.
34. Dubash SR, Merchant S, Heinzmann K, Mauri F, Lavdas I, Inglese M, Kozlowski K, Rama N, Masrour N, Steel JF, Thornton A, Lim AK, Lewanski C, Cleator S, Coombes RC, Kenny L, Aboagye EO. Clinical translation of [¹⁸F] ICMT-11 for measuring chemotherapy-induced caspase 3/7 activation in breast and lung cancer. *Eur J Nucl Med Mol Imaging*. 2018;45:2285–99.
35. Jouberton E, Schmitt S, Chautard E, Maisonia-Besset A, Roy M, Radosevic-Robin N, Chezal JM, Miot-Noirault E, Bouvet Y, Cachin F. [¹⁸F]ML-10 PET imaging fails to assess early response to neoadjuvant chemotherapy in a preclinical model of triple negative breast cancer. *EJNMMI Res*. 2020;10:2.
36. Elvas F, Vangestel C, Pak K, Vermeulen P, Gray B, Stroobants S, Staelens S, Wyffels L. Early prediction of tumor response to treatment: preclinical validation of 99mTc-Duramycin. *J Nucl Med*. 2016;57:805–11.
37. Elvas F, Boddaert J, Vangestel C, Pak K, Gray B, Kumar-Singh S, Staelens S, Stroobants S, Wyffels L. ^{99m}Tc-Duramycin SPECT imaging of early tumor response to targeted therapy: a comparison with ¹⁸F-FDG PET. *J Nucl Med*. 2017;58:665–70.
38. Johnson SE, Ugolkov A, Haney CR, Bondarenko G, Li L, Waters EA, Bergan R, Tran A, O'Halloran TV, Mazar A, Zhao M. Whole-body imaging of cell death provides a systemic, minimally invasive, dynamic, and near-real time indicator for chemotherapeutic drug toxicity. *Clin Cancer Res*. 2019;25:1331–42.
39. Rix A, Drude NI, Mrugalla A, Baskaya F, Pak KY, Gray B, Kaiser HJ, Tolba RH, Fiegle E, Lederle W, Mottaghy FM, Kiessling F. Assessment of chemotherapy-induced organ damage with Ga-68 labeled Duramycin. *Mol Imaging Biol*. 2020;22:623–33.
40. Elvas F, Vangestel C, Rapic S, Verhaeghe J, Gray B, Pak K, Stroobants S, Staelens S, Wyffels L. Characterization of [(99m)Tc]Duramycin as a SPECT imaging agent for early assessment of tumor apoptosis. *Mol Imaging Biol*. 2015;17:838–47.
41. Yagle KJ, Eary JF, Tait JF, Grierson JR, Link JM, Lewellen B, Gibson DF, Krohn KA. Evaluation of 18F-annexin V as a PET imaging agent in an animal model of apoptosis. *J Nucl Med*. 2005;46:658–66.
42. Davis DW, Buchholz TA, Hess KR, Sahin AA, Valero V, McConkey DJ. Automated quantification of apoptosis after neoadjuvant chemotherapy for breast cancer: early assessment predicts clinical response. *Clin Cancer Res*. 2003;9:955–60.
43. Mohsin SK, Weiss HL, Gutierrez MC, Chamness GC, Schiff R, Digiovanna MP, Wang CX, Hilsenbeck SG, Osborne CK, Allred DC, Elledge R, Chang JC. Neoadjuvant trastuzumab induces apoptosis in primary breast cancers. *J Clin Oncol*. 2005;23:2460–8.
44. Wan C, Kiessling V, Cafiso DS, Tamm LK. Partitioning of synaptotagmin I C2 domains between liquid-ordered and liquid-disordered inner leaflet lipid phases. *Biochemistry*. 2011;50:2478–85.
45. Larkin TJ, Canuto HC, Kettunen MI, Booth TC, Hu DE, Krishnan AS, Bohndiek SE, Neves AA, McLachlan C, Hobson MP, Brindle KM. Analysis of image heterogeneity using 2D Minkowski functionals detects tumor responses to treatment. *Magn Reson Med*. 2014;71:402–10.
46. Piron S, De Man K, Van Laeken N, D'Asseler Y, Bacher K, Kersemans K, Ost P, Decaestecker K, Deseyne P, Fonteyne V, Lumen N, Achten E, Brans B, De Vos F. Radiation dosimetry and biodistribution of ¹⁸F-PSMA-11 for PET imaging of prostate cancer. *J Nucl Med*. 2019;60:1736–42.
47. Kemerink GJ, Liem IH, Hofstra L, Boersma HH, Buijs WC, Reutelingsperger CP, Heidendal GA. Patient dosimetry of intravenously administered ^{99m}Tc-annexin V. *J Nucl Med*. 2001;42:382–7.
48. Quinn B, Dauer Z, Pandit-Taskar N, Schoder H, Dauer LT. Radiation dosimetry of 18F-FDG PET/CT: incorporating exam-specific parameters in dose estimates. *BMC Med Imaging*. 2016;16:41.

Publisher's Note

Springer Nature remains neutral with regard to jurisdictional claims in published maps and institutional affiliations.

Submit your manuscript to a SpringerOpen® journal and benefit from:

- Convenient online submission
- Rigorous peer review
- Open access: articles freely available online
- High visibility within the field
- Retaining the copyright to your article

Submit your next manuscript at ► [springeropen.com](https://www.springeropen.com)
